GEOPHYSICS, VOL. 77, NO. 2 (MARCH-APRIL 2012); P. J1–J5, 5 FIGS.
10.1190/GEO2011-0425.1

3D migration for rapid imaging of total-magnetic-intensity data

Michael S. Zhdanov[1], Xiaojun Liu[2], Glenn A. Wilson[3], and Le Wan[1]

ABSTRACT

Three-dimensional potential field migration for rapid imaging of entire total-magnetic-intensity (TMI) surveys is introduced, and real time applications are discussed. Potential field migration is based on a direct integral transformation of the measured TMI data into a 3D susceptibility model, which could be directly used for interpretation or as an a priori model for subsequent regularized inversion. The advantage of migration is that it does not require any a priori information about the type of the sources present, nor does it rely on regularization as per inversion. Migration is very stable with respect to noise in measured data because the transform is reduced to the downward continuation of a function that is analytical everywhere in the subsurface. The 3D migration of TMI data acquired over the Reid-Mahaffy test site in Ontario, Canada is used as a test study. Our results are shown to be consistent with those results obtained from 3D regularized inversion as well as the known geology of the area. Interestingly, the migration of raw TMI data produces results very similar to the inversion of diurnally corrected and microleveled TMI data, suggesting that migration could be applied directly to real-time imaging during the acquisition.

INTRODUCTION

The earth's magnetic field is the vector sum of contributions from two main sources: a background field due to the dynamo effect of the earth's liquid core, and anomalous fields due to magnetic rocks and minerals above the Curie isotherm. Magnetic vector data, measured by orthogonal fluxgate magnetometers, are dominated by the earth's background field and are thus very sensitive to instrument orientation. The development of reliable and low-cost optically pumped magnetometers in the 1960s enabled direct measurement of the total magnetic intensity (TMI), regardless of instrument orientation. It is now routine practice that every airborne geophysical survey produces TMI data as a standard deliverable.

Relative to the millions of line-kilometers of TMI data acquired each year during early stages of exploration, 3D inversions are rarely performed. This is a reflection of the limited capability of existing 3D inversion software to invert entire surveys to relevant 3D earth models with sufficient resolution in sufficient time so as to affect exploration decisions. At their simplest, interpretations are based on picking lineaments from the maps of the first vertical derivative of the TMI. Structural interpretations are usually based on some kind of Euler deconvolution, eigenvector, wavelet, analytic signal, or depth-from-extreme-points methods (e.g., Nabighian et al., 2005). We present an alternative method of rapid 3D imaging based on the principles of potential field migration as originally introduced by Zhdanov (2002). The advantage of 3D migration is that it does not require any a priori information about the type of the sources, nor does it rely on regularization as per 3D inversion. In Zhdanov et al. (2011), 3D potential field migration was developed for gravity and gravity gradiometry. In this letter, we extend the concept to 3D potential field migration of TMI data for a 3D susceptibility distribution.

Mathematically, migration is the action of an adjoint operator on the observed data. This concept has long been developed for seismic and electromagnetic wavefields, where the adjoint operators manifest themselves as the (backward) propagation of seismic or electromagnetic fields in reverse time (Claerbout, 1985; Tarantola, 1987; Zhdanov, 1988, 2002). When applied to potential fields such as gravity or magnetics, migration manifests itself as a downward continuation of the migration field, which is obtained by relocating the sources of the observed field into the upper half-space as mirror images of the true sources (Figure 1) (e.g., Zhdanov et al., 2011). We note that the downward continuation of the measured TMI field and the migration TMI field are significantly different. The downward continuation of the measured TMI field has singularities in the lower half-space associated with its sources, so its downward continuation can only be extended down to those singular points,

Manuscript received by the Editor 22 October 2011; revised manuscript received 26 December 2011; published online 8 March 2012.
[1]University of Utah, Department of Geology and Geophysics, Salt Lake City, Utah, USA and TechnoImaging, Salt Lake City, Utah, USA. E-mail: mzhdanov@technoimaging.com; le@technoimaging.com.
[2]University of Utah, Department of Geology and Geophysics, Salt Lake City, Utah, USA. E-mail: xiaojun.liu@utah.edu.
[3]TechnoImaging, Salt Lake City, Utah, USA. E-mail: glenn@technoimaging.com.
© 2012 Society of Exploration Geophysicists. All rights reserved.

Downloaded 19 Mar 2012 to 155.101.18.163. Redistribution subject to SEG license or copyright; see Terms of Use at http://segdl.org/

making it an ill-posed and unstable transform (e.g., Strakhov, 1970; Zhdanov, 1988). The migration TMI field has singular points in the upper half-space; therefore, its downward continuation is a well-posed and stable transform away from the mirror images of the sources, and thus, avoids singularities. At the same time, the migration field does contain remanent information about the original source distribution, which is why it can be used for imaging.

ADJOINT OPERATOR FOR THE TOTAL MAGNETIC INTENSITY

We have measured TMI data on a surface S above a domain V that is filled by magnetic sources with the intensity of magnetization $\mathbf{I}(\mathbf{r})$. There are no restrictions on either the surface or the domain. The problem is to determine the magnetic susceptibility $\chi(\mathbf{r})$. In what follows, we adopt the common assumptions that there is no remanent magnetization, that the self-demagnetization effect is negligible, and that the magnetic susceptibility is isotropic (e.g., Li and Oldenburg, 1996; Portniaguine and Zhdanov, 2002). Under such assumptions, the intensity of magnetization is linearly related to an inducing magnetic field $\mathbf{H}^0(\mathbf{r})$through the magnetic susceptibility

$$\mathbf{I}(\mathbf{r}) = \chi(\mathbf{r})\mathbf{H}^0(\mathbf{r}) = \chi(\mathbf{r})H^0\mathbf{l}(\mathbf{r}), \tag{1}$$

where H^0 is the magnitude of the inducing field, $\mathbf{l}$ is a unit vector in the direction of magnetization, and $\mathbf{r}$ is the radius vector of a point

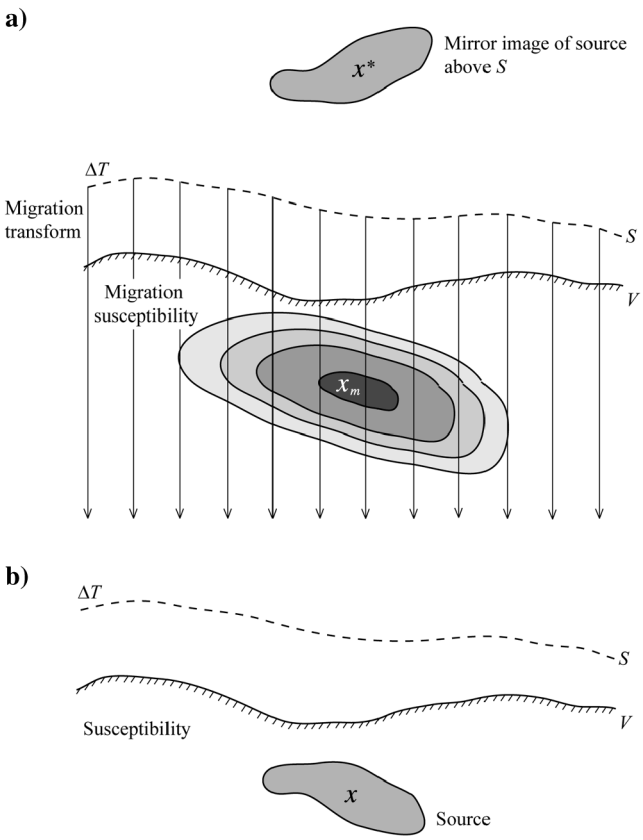

Figure 1. (a) The migration susceptibility χ_m is obtained from the migration transform of the anomalous TMI data ΔT away from the mirror image above the surface S of the susceptibility distribution χ^*. (b) Anomalous TMI data ΔT measured on a surface S are due to a susceptibility distribution χ inside a domain V.

within the domain V. The inducing magnetic field is assumed constant over the survey area.

It is well known that the anomalous TMI data ΔT generated by the magnetic sources within the volume V can be represented by the linear operator equation (Zhdanov, 1998),

$$\Delta T(\mathbf{r}') = A(\chi) = H^0 \iiint_V \frac{\chi(\mathbf{r})}{|\mathbf{r}-\mathbf{r}'|^3} K(\mathbf{r}'-\mathbf{r})dv, \tag{2}$$

where K is the TMI kernel:

$$K(\mathbf{r}'-\mathbf{r}) = \frac{3(\mathbf{l}\cdot(\mathbf{r}'-\mathbf{r}))^2}{|\mathbf{r}'-\mathbf{r}|^2} - 1. \tag{3}$$

We introduce a real Hilbert space D of data with the metric

$$(f,g)_D = \iint_S f(\mathbf{r}')g(\mathbf{r}')ds'; \qquad f,g \in D \tag{4}$$

and also introduce a real Hilbert space M of models (i.e., magnetic susceptibility χ) with the metric

$$(\chi,\eta)_M = \iiint_V \chi(\mathbf{r})\eta(\mathbf{r})dv; \qquad \chi,\eta \in M. \tag{5}$$

According to definition, the adjoint operator $A^\star$satisfies to the following equation:

$$(A(\chi),f)_D = (\chi, A^\star(f))_M. \tag{6}$$

Following Zhdanov (2002), one can solve equation 6 and find the explicit form of the Hermitian adjoint operator $A^\star$as applied to any function $f(\mathbf{r}')$:

$$A^\star(f) = H^0 \iint_S \frac{f(\mathbf{r}')}{|\mathbf{r}'-\mathbf{r}|^3} K(\mathbf{r}'-\mathbf{r})ds'. \tag{7}$$

We note that the TMI adjoint operator produces a function that is analytical everywhere in the subsurface. The significance of this will become apparent momentarily.

MIGRATION OF THE TOTAL MAGNETIC INTENSITY

Mathematically, migration is the action of the adjoint operator on the observed data (Tarantola, 1987; Zhdanov, 1988, 2002). It follows that the migration TMI field $\Delta T^m(\mathbf{r})$ is introduced as the action of the TMI adjoint operator $A^\star$ on the measured TMI field ΔT:

$$\Delta T^m(\mathbf{r}) = A^\star \Delta T. \tag{8}$$

We note, however, that direct migration of the measured TMI field does not produce an adequate image of the susceptibility distribution because the migration fields rapidly attenuate with the depth. Similar to spatial weighting in 3D regularized inversion (e.g., Li and Oldenburg, 1996; Portniaguine and Zhdanov, 2002), one should apply an appropriate spatial weighting operator to the migration TMI field to image the sources at their correct locations. Similar to 3D gravity migration (Zhdanov et al., 2011), the migration susceptibility can be computed from

$$\chi^m(\mathbf{r}) = k(W^\star W)^{-1}A^\star \Delta T = kw^{-2}(z)\Delta T^m(\mathbf{r}). \tag{9}$$

Downloaded 19 Mar 2012 to 155.101.18.163. Redistribution subject to SEG license or copyright; see Terms of Use at http://segdl.org/

In the last formula, the unknown coefficient k can be determined by a linear line search according to

$$k = \frac{\|A^{w\star}\Delta T\|_M^2}{\|A^w A^{w\star}\Delta T\|_D^2}, \tag{10}$$

where

$$A^w = AW^{-1} \tag{11}$$

and the linear weighting operator W is selected as an operator of multiplication of the susceptibility χ by a depth-weighting function w, which is equal to the square root of the integrated sensitivity $a(z)$ of the TMI data (Zhdanov, 2002):

$$w(z) = \sqrt{\frac{\|\delta\Delta T^{\text{obs}}\|_D}{\delta\chi}} = \sqrt{a(z)}, \tag{12}$$

which is independent of the source and may be evaluated analytically.

Substituting equations 8 and 12 into equation 9, we find that

$$\chi^m(\mathbf{r}) = \frac{kH^0}{a(z)} \iint_S \frac{\Delta T(\mathbf{r}')}{|\mathbf{r}' - \mathbf{r}|^3} K(\mathbf{r} - \mathbf{r}')ds'. \tag{13}$$

The migration magnetic susceptibility 13 is proportional to the magnitude of the weighted migration field $\Delta T^m(\mathbf{r})$, which is analytical everywhere in the subsurface, implying that migration is a well-posed and stable transform. It can be shown that if the surface S coincides with the horizontal axis $z = 0$, migration is mathematically equivalent to a form of downward continuation of a function analytical everywhere in the lower half-space. Equation 13 can be identified as a Fredholm equation of the first kind because the migration TMI field is a weighted average of all TMI data from the surface S where the TMI kernel is the weighting function. This is a smoothing operation, and thus we can reasonably expect migration to produce smooth susceptibility models similar to smooth regularized inversion. This also means migration has similar limitations as per smooth inversion, particularly the inability to recover sharp contrasts. Migration is a transform of the anomalous TMI data, so one disadvantage is that the susceptibility model does not reproduce the anomalous TMI data in a least-square sense. However, it is possible to apply migration iteratively to residual fields, and this would be equivalent to regularized inversion (e.g., Zhdanov, 2002).

MODEL STUDY

To investigate the performance of 3D TMI migration, we have considered two discrete bodies with susceptibility of 0.05 (SI units) buried about 110 m below variable topography (Figure 2a). The inducing field had an inclination of 75° and declination of 25°. The synthetic TMI data were computed on a 20-m regular grid draped over a variable surface covering an area of one square kilometer. Figure 2b shows an example of a profile of the TMI data over both bodies. We have applied 3D migration to the entire synthetic TMI data set and calculated the migration magnetic susceptibility according to equation 13. It is important to point out that the migration was performed on data acquired on a variable observation surface. As an example, Figure 2c shows a vertical cross section through the 3D migration magnetic

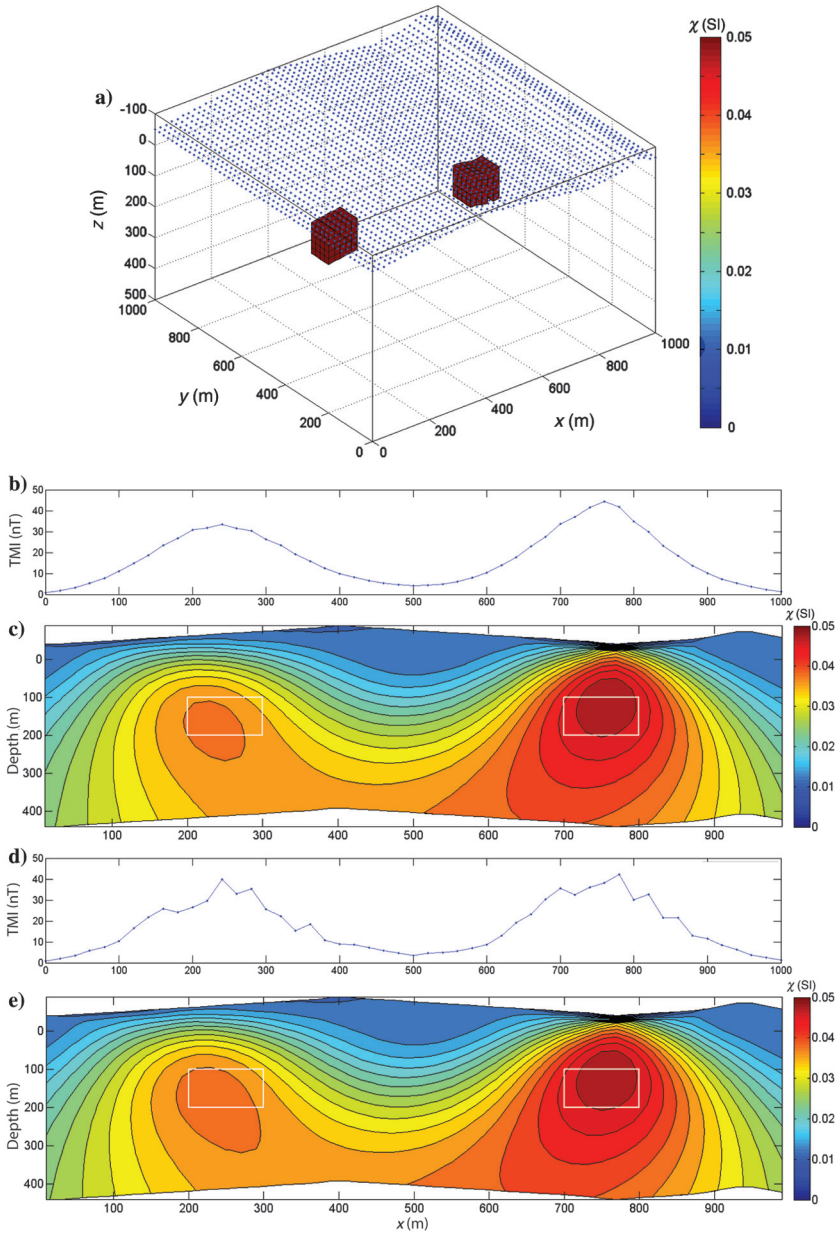

Figure 2. (a) Perspective of 3D model consisting of two blocks of 0.05 (SI) susceptibility. Observation sites (blue) are located across a variable topography. (b) Synthetic TMI data along the profile $y = 500$ m. (c) Vertical cross section of susceptibility along $y = 500$ m, which crosses the centers of the bodies, from 3D migration of synthetic TMI data. (d) Synthetic TMI data with 20% random Gaussian noise along the profile $y = 500$ m. (e) Vertical cross section of susceptibility along $y = 500$ m from 3D migration of noisy synthetic TMI data. The white boxes show the true positions of the bodies.

Downloaded 19 Mar 2012 to 155.101.18.163. Redistribution subject to SEG license or copyright; see Terms of Use at http://segdl.org/

susceptibility model. The correct locations of the two bodies' centers can be determined. To demonstrate the robustness of migration to noise, we contaminated the data with 20% random Gaussian noise, as shown in Figure 2d. Figure 2e shows the same vertical cross section of results for the 3D migration of the noisy data. As expected, 3D migration produces a very robust image of the susceptibility distribution. Note that this model is representative of simple mineral or engineering targets. More complex models should be considered in a case of hydrocarbon exploration. Some examples of detailed study of migration for the gravity gradiometry data can be found in Zhdanov

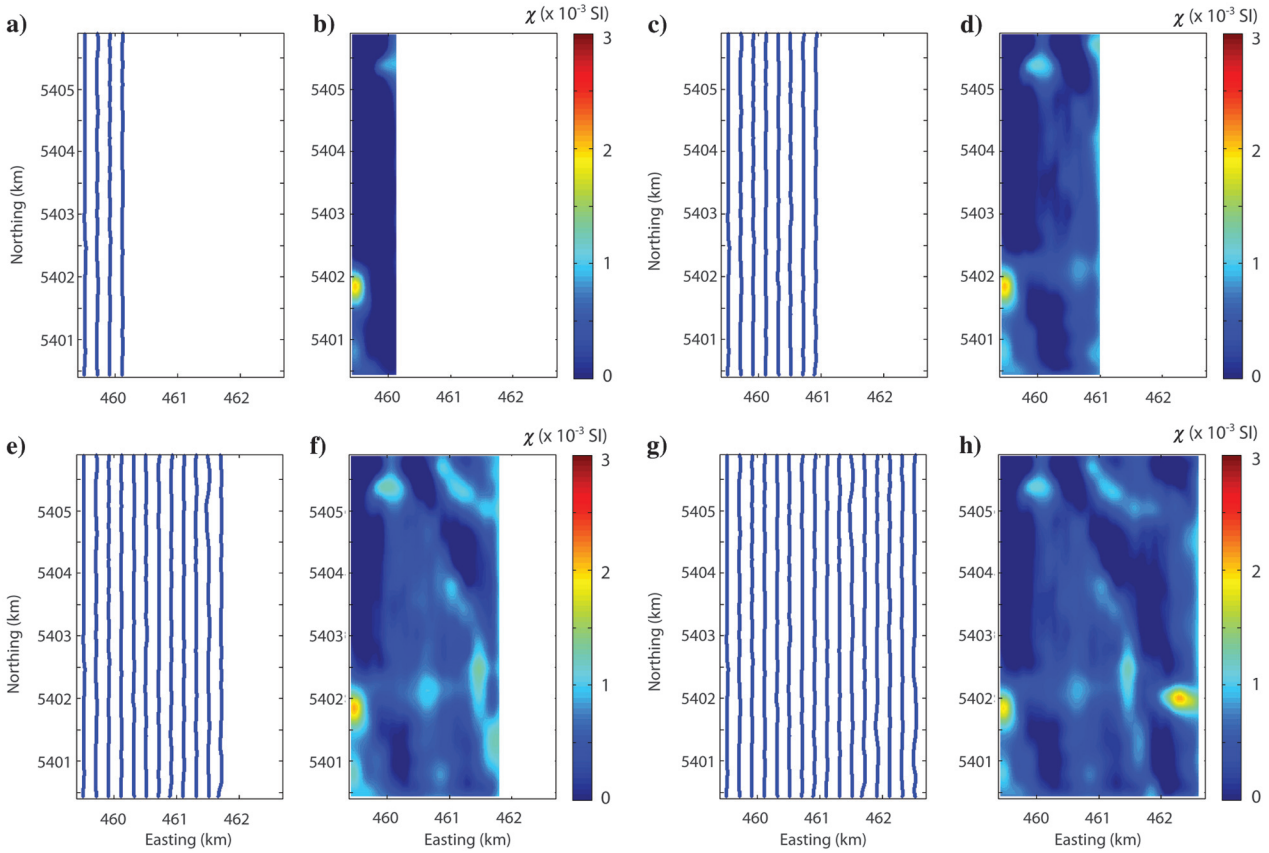

Figure 3. Simulation of real-time imaging during acquisition for an airborne TMI survey from the Reid-Mahaffy test site with (a and b) four , (c and d) eight, (e and f) 12, and (g and h) 16 survey lines; horizontal cross sections of the magnetic susceptibility are shown for 100 m depth.

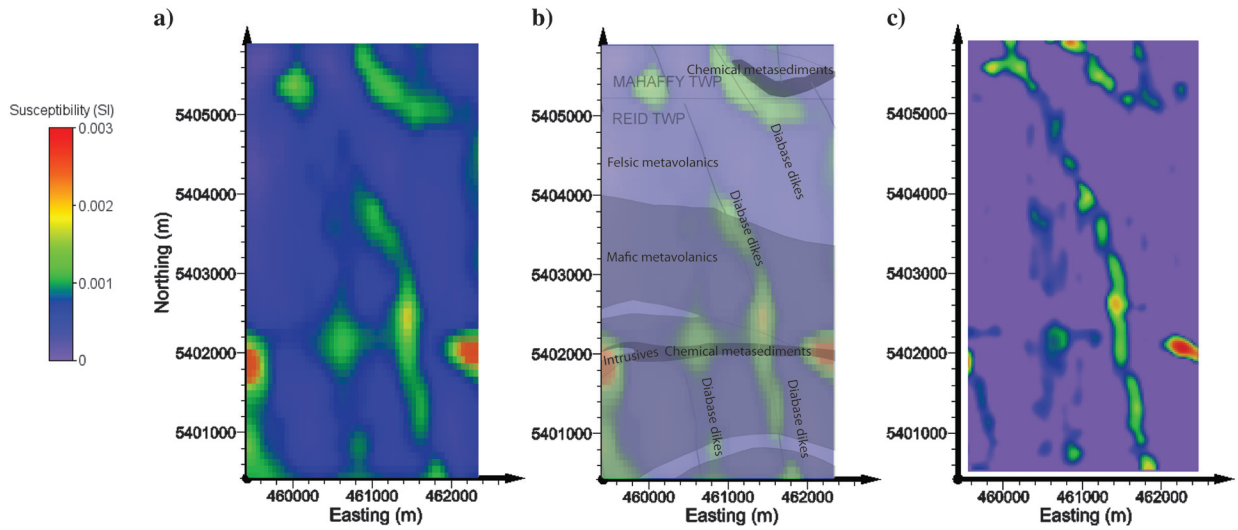

Figure 4. (a) Horizontal cross section of susceptibility at 100 m depth from the 3D migration of the Reid-Mahaffy anomalous raw TMI data; (b) with geology overlain (courtesy of Ontario Geological Survey); and (c) horizontal cross section of susceptibility at 100 m depth from the 3D regularized inversion of the Reid-Mahaffy anomalous processed TMI data.

Downloaded 19 Mar 2012 to 155.101.18.163. Redistribution subject to SEG license or copyright; see Terms of Use at http://segdl.org/

et al. (2011), where it is shown that the bodies separated by a small distance are difficult to resolve. We also note that due to nonuniqueness of potential fields, stacked sources are difficult to resolve.

CASE STUDY — REID-MAHAFFY

The Reid-Mahaffy test site is located north of Timmins on the border of the Reid and Mahaffy townships in Ontario, Canada, and is representative of Archean terranes. It is located in the Abitibi Subprovince, immediately east of the Mattagami River Fault. The area is underlain by Archean (~2.7 billion years) mafic to intermediate metavolcanic rocks in the south and felsic to intermediate metavolcanic rocks in the north, with a roughly east–west-striking stratigraphy. Narrow horizons of chemical metasedimentary rocks and felsic metavolcanic rocks have been mapped as well as a mafic-to-ultramafic intrusive suite to the southeast. Copper and lead-zinc vein/replacement and stratabound volcanogenic massive sulfide (VMS) mineralization occurs in the immediate vicinity. For example, the Kidd Creek VMS deposit occurs to the southeast of the survey area (Ontario Geological Survey, 2000).

At approximately 90 line km, the survey area is very small for an airborne survey. However, the presence of weakly magnetic north–northwest-striking Proterozoic diabase dikes with anomalous TMI of several hundred nanoteslas make the site ideal for demonstration of our 3D TMI migration. We consider the TMI data acquired as part of an AEROTEM™ survey. The survey lines are shown in the left panels of Figure 3. We removed the magnitude of the IGRF from the raw TMI data and sequentially applied the 3D migration to the anomalous raw TMI data from four, eight, 12, and 16 lines, as shown in Figure 3a, 3c, 3e, and 3g, respectively. The flight lines were approximately 6 km long and 200 m apart, and the data were acquired over a variable surface. The right panels of Figure 3 show the temporal evolution of the 3D susceptibility model at 100 m depth during this simulated airborne acquisition. One can see how the image evolves from just a small section on the east part of the survey area to ultimately include the entire survey area.

The IGRF background field was then removed from the diurnally corrected and microleveled (i.e., processed) TMI data. We then performed 3D regularized inversion on the anomalous processed TMI data, using the algorithm described by Wilson et al. (2011). Figure 4 shows the horizontal cross sections of the magnetic susceptibility at 100 m depth. As expected, we can clearly see the lateral shape and extent of the diabase dikes (Figure 4b). We also note that migration of the anomalous raw TMI data captures the same structures as per 3D inversion of the anomalous processed TMI data (Figure 4c). A perspective of the 3D susceptibility model obtained from TMI migration is shown in Figure 5. We note that a single iteration of 3D migration runs several orders of magnitude faster than regularized inversion, and this suggests that 3D migration could be applied to real-time imaging.

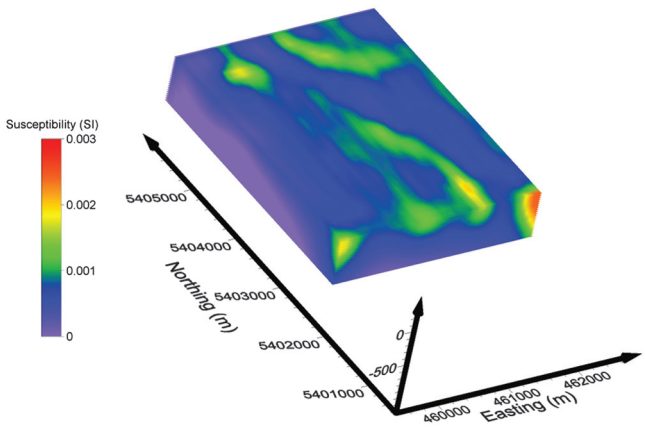

Figure 5. Perspective of the 3D TMI migration from the Reid-Mahaffy test site.

CONCLUSIONS

We have introduced 3D potential field migration for the rapid 3D imaging of TMI data. The method is based on a direct integral transformation of the measured TMI data into a 3D susceptibility model. The advantage of 3D TMI migration is that it does not require any a priori information about the type of the sources present, nor does it rely on regularization as per 3D inversion. Three-dimensional TMI migration is very stable with respect to noise in the measured TMI data because the transform is reduced to the downward continuation of a function that is analytical everywhere in the lower half-space. Interestingly, the migration of raw TMI data produces results very similar to the 3D regularized inversion of diurnally corrected and microleveled TMI data, suggesting that migration can be applied directly to real-time 3D imaging during TMI acquisition.

ACKNOWLEDGMENTS

The authors acknowledge TechnoImaging for support of this research and permission to publish. Zhdanov, Liu, and Wan also acknowledge support of the University of Utah's Consortium for Electromagnetic Modeling and Inversion (CEMI). The Reid-Mahaffy TMI data were provided by AeroQuest. The authors thank Martin Čuma of TechnoImaging and the University of Utah's Center for High Performance Computing (CHPC) for providing the Reid-Mahaffy 3D TMI inversions. The authors also thank Associate Editor Kasper van Wijk, and reviewers Fabio Caratori Tontini, Partha Routh, and Ed Biegert for their suggestions, which improved the manuscript.

REFERENCES

Claerbout, J. F., 1985, Imaging the earth's interior: Blackwell Scientific Publications.

Li, Y., and D. W. Oldenburg, 1996, 3D inversion of magnetic data: Geophysics, **61**, 394–408, doi: 10.1190/1.1443968.

Nabighian, M. N., V. J. S. Grauch, R. O. Hansen, T. R. LaFehr, Y. Li, J. W. Peirce, J. D. Phillips, and M. E. Ruder, 2005, The historical development of the magnetic method in exploration: Geophysics, **70**, no. 6, 3ND–61ND, doi: 10.1190/1.2133784.

Ontario Geological Survey, 2000, Airborne magnetic and electromagnetic surveys, Reid-Mahaffy airborne geophysical test site Survey: Ontario Geological Survey, Miscellaneous Release — Data (MRD)-55.

Portniaguine, O., and M. S. Zhdanov, 2002, 3D magnetic inversion with data compression and image focusing: Geophysics, **67**, 1532–1541, doi: 10.1190/1.1512749.

Strakhov, V. N., 1970, Some aspects of the plane inverse problem of magnetic potential (in Russian): Izvestiya Akademii Nauk SSSR Fizika Zemli, **9**, 31–41.

Tarantola, A., 1987, Inverse problem theory: Elsevier.

Wilson, G. A., M. Čuma, and M. S. Zhdanov, 2011, Massively parallel 3D inversion of gravity and gravity gradiometry data: Preview (Magazine of the Australian Society of Exploration Geophysicists), no. 152, 29–34, doi: 10.1071/PVv2011n152p29.

Zhdanov, M. S., 1988, Integral transforms in geophysics: Springer-Verlag.

Zhdanov, M. S., 2002, Geophysical inverse theory and regularization problems: Elsevier.

Zhdanov, M. S., X. Liu, G. A. Wilson, and L. Wan, 2011, Potential field migration for rapid imaging of gravity gradiometry data: Geophysical Prospecting, **59**, no. 6, 1052–1071, doi: 10.1111/gpr.2011.59.issue-6.

Downloaded 19 Mar 2012 to 155.101.18.163. Redistribution subject to SEG license or copyright; see Terms of Use at http://segdl.org/